Spectrochimica Acta Part A: Molecular and Biomolecular Spectroscopy 159 (2016) 21–29

Contents lists available at ScienceDirect

Spectrochimica Acta Part A: Molecular and Biomolecular Spectroscopy

journal homepage: www.elsevier.com/locate/saa

A micro-Raman spectroscopic investigation of leukemic U-937 cells in aged cultures

Enza Fazio [a], Sebastiano Trusso [b], Domenico Franco [c,*], Marco Sebastiano Nicolò [c], Alessandro Allegra [d], Fortunato Neri [a], Caterina Musolino [d], Salvatore P.P. Guglielmino [c]

[a] Dipartimento di Scienze Matematiche e Informatiche, Scienze Fisiche e Scienze della Terra, University of Messina, Viale F. Stagno d'Alcontres 31, 98166 Messina, Italy
[b] CNR-IPCF Istituto per i Processi Chimico-Fisici, Viale F. Stagno d'Alcontres 37, 98158 Messina, Italy
[c] Dipartimento di Scienze Chimiche, Biologiche, Farmaceutiche ed Ambientali, University of Messina, Viale F. Stagno d'Alcontres 31, 98166 Messina, Italy
[d] Dipartimento di Patologia Umana dell'adulto e dell'età Evolutiva "Gaetano Barresi", University of Messina, Via Consolare Valeria, 1, 98125 Messina, Italy

ARTICLE INFO

Article history:
Received 29 October 2015
Received in revised form 13 January 2016
Accepted 20 January 2016
Available online 21 January 2016

Keywords:
U397 neoplastic cells
Micro-Raman technique
Multivariate data analysis
Single cells identification

ABSTRACT

Recently it has been shown that micro-Raman spectroscopy combined with multivariate analysis is able to discriminate among different types of tissues and tumoral cells by the detection of significant alterations and/or reorganizations of complex biological molecules, such as nucleic acids, lipids and proteins. Moreover, its use, being in principle a non-invasive technique, appears an interesting clinical tool for the evaluation of the therapeutical effects and of the disease progression. In this work we analyzed molecular changes in aged cultures of leukemia model U937 cells with respect to fresh cultures of the same cell line. In fact, structural variations of individual neoplastic cells on aging may lead to a heterogeneous data set, therefore falsifying confidence intervals, increasing error levels of analysis and consequently limiting the use of Raman spectroscopy analysis. We found that the observed morphological changes of U937 cells corresponded to well defined modifications of the Raman contributions in selected spectral regions, where markers of specific functional groups, useful to characterize the cell state, are present. A detailed subcellular analysis showed a change in cellular organization as a function of time, and correlated to a significant increase of apoptosis levels. Besides the aforementioned study, Raman spectra were used as input for principal component analysis (PCA) in order to detect and classify spectral changes among U937 cells.

© 2016 Elsevier B.V. All rights reserved.

1. Introduction

Recognition of altered cells and the correct identification of the different stages of sporadic tumor cells is one of the principal objectives in biomedical field. The effectiveness of targeted cancer therapies, in fact, depends not only on the initial tumor discrimination but also on its evolution that can result from clonal expansion, genetic diversification and clonal selection as a consequence of chemotherapy [1]. In such a case, cancer progression can enhance the levels of morphological, anatomical and molecular heterogeneity in neoplastic cells.

Since Raman spectroscopy provides a fingerprint of molecules, it can be used to recognize specific cancer cell changes that take place in nucleic acids, proteins, lipids and carbohydrate quantities and/or conformation [2]. Moreover, being a non-invasive technique allows data acquisition in vitro at a single-cell level in an exogenous label-free way [3,4]. Many research teams have therefore focused their research to the development of sensitive assays to detect single tumor cells. For instance, in a pilot research micro-Raman imaging was used to identify rare disseminated tumor cells circulating in the human peripheral blood [5], other studies proved the ability to differentiate breast (BT 549) and colorectal (HCT 116) circulating tumor cells with respect to human mononuclear cells [6]. Although Raman spectroscopy can be, in principle, applied for in vitro diagnosis, several issues still limit its use on a large scale and, even more, in routine clinical testing. Currently, the main limitation consists in the classification and interpretation of the spectral data, when structural variations of neoplastic cells occur as a consequence of cancer development and progression. In such a case, the analysis process can be significantly improved by the use of statistical multivariate methods such as principal component analysis (PCA) and hierarchical clusters analysis (HCA). These methods are able to outline subtle spectral differences among the Raman spectra and hence to classify cellular systems.

However, processing raw (as obtained) spectral data by statistical methods has its disadvantages: subtle variances of spectra can occur within the same cell line and coupled with the experimental noise lead to an intrinsic poor spectra reproducibility and to a low statistical

* Corresponding author at: Dipartimento di Scienze Chimiche, Biologiche, Farmaceutiche ed Ambientali, Viale F. Stagno d'Alcontres 31, 98166 Messina, Italy.
E-mail address: dfranco@unime.it (D. Franco).

http://dx.doi.org/10.1016/j.saa.2016.01.032
1386-1425/© 2016 Elsevier B.V. All rights reserved.

analysis confidence level. In such cases, refined pre-treatment data procedures are needed to improve PCA discrimination analysis, as for example, a second derivative-based PCA approach, which makes possible selective cell line recognition and spectra reproducibility [7]. Such an approach has proven reliable only for statistical analysis carried out on a large cells number, belonging either to the same or to different cellular lines.

A deep and detailed analysis of Raman spectral regions is needed when a limited number of cells is available, even more when the individual variability of some cells has to be considered, such as in the case of minimal residual disease, e.g. tumor cells variation due to therapeutic treatments or, more simply, lifetime cells structural variation. In a given cell line, normal metabolic cell processes lead to detectable Raman spectral changes: dividing cells, as an example, show a typical staining pattern and characteristic variations in the amide I and II Raman spectral contributions. Similar changes are observed when cells progress through the G1, S and G2 phases, [8] or in apoptotic and necrotic stage [9].

Despite these difficulties, we will show in this paper that it is still possible to screen and to label the evolution of highly variable cancer cells by micro-Raman spectroscopy, and to quantify biochemical alterations in U937 malignant cells before and after aging.

U937 cellular line was chosen as a leukemia model, it shows many monocytic characteristics, such as differentiation or apoptosis susceptibility, cytokine secretion phenomena and new receptors exhibition. To highlight Raman spectra dependence on the cellular state, measurements were carried out on U937 cells cultured for 24 and 144 h. In fact, it has been proposed that oxidative stress leads to DNA damage, with the consequent accumulation of mutations, genomic instability, loss of function and apoptosis. PCA barcode analysis was used to identify Raman spectra belonging to similar cells stages, while single cell analysis was carried out to identify metabolic changes correlated to Raman peaks intensity variations. The obtained results open up new perspectives in monitoring the different metabolic state of sporadic tumor cells occurring naturally or after chemotherapeutic treatments.

2. Materials and methods

2.1. U937 cell line and culture conditions

U937 is a human cell line established from a diffuse histiocytic lymphoma [10]. U937 cell line was purchased from American Type Culture Collection (ATCC® CRL-1593.2™, Milan, Italy) and maintained in RPMI 1640 with L-Glutamine (Lonza, Basel, Switzerland) supplemented with 10% fetal bovine serum (FBS, Lonza, Basel, Switzerland), penicillin (100 units/mL) and streptomycin (100 μg/mL) at 37 °C in humidified 5% CO_2 incubator. After transferring into fresh culture vessels, cell lines of the same lot were cultured for 24 and 144 h in complete growth medium.

2.2. Preparation protocol for cells characterization

Before Raman spectroscopic analysis, samples by each cell culture were stained with Trypan Blue (Sigma-Aldrich, Milan, Italy) and DAPI (Sigma-Aldrich, Milan, Italy), to measure the average number of non-viable cells and to detect necrotic cells from those undergoing apoptosis.

The U937 cell line (at cell density between 1×10^5 and 2×10^6 viable cells/mL), were centrifuged at 500 $\times g$ for 5 min and washed twice in Phosphate Buffer Saline (PBS, Sigma-Aldrich, Milan, Italy). Finally, 50 μL of cell suspension were deposed on a CaF_2 slide, previously cleaned in methanol, for greasy or waxy contaminants, and treated with 0.01% polylysine (Sigma-Aldrich, Milan, Italy). Each sample was fixed by air-dried fixation in sterile condition for 15 min. All tests were performed in triplicate.

Raman scattering measurements were carried out by means of Horiba XploRA micro-Raman spectrometer using the 532 nm laser line, focused on the sample's surface through the 100× objective of a microscope. The backscattered radiation was collected by the same microscope optics and dispersed by a monochromator equipped with a 600 line/mm holographic grating. The dispersed radiation was detected by means of a Peltier-cooled charged-coupled device (CCD) sensor. In order to avoid cells damaging, the laser power at the sample surface was kept as low as possible (≈1 mW), while the integration and the accumulation times were fixed at 50 s and 3 s, respectively. Cells showed no detectable damage. For each sample, Raman analyses were randomly performed on a low number of cells (30–35 cells). It's worth to report that the laser spot dimension of about 1 μm^2, smaller than the typical cell dimension, was located at different regions of the glass slide.

2.3. Variance analysis

Spectra of each cell line were individually normalized to their proper area in order to minimize fluctuations due to signal intensity variations. The mean spectrum was calculated and the most significant bands identified. In order to obtain information about cell line homogeneity, a variance analysis of spectral intensities was carried out. Standard deviation of individual Raman peaks intensity, with respect to the mean value, was calculated and given in %.

2.4. Single cell analysis

In order to point out possible morphological and nuclear alterations, cells taken from the same samples were separately evaluated by optical and epifluorescence microscopy. Samples for optical microscopy were prepared following the protocol used in micro-Raman analysis. Differently, cells for image analysis by epifluorescence microscopy were prepared as follows: cells were centrifuged and washed in PBS buffer, therefore stained with DAPI at 0.1 μg/mL in PBS at 30 °C for 15–30 min [11]. DAPI stained cells were observed by Leica DMRE epifluorescence microscope with Leica C Plan 63× objective, using a BP 340–380 nm excitation filter in combination with a LP 425 nm suppression filter. In order to evaluate intracellular variability, after acquiring an image of the cells, Raman scattering measurements were performed, repositioning laser spots onto three different regions within the cell. We remember that U937 cells volume is occupied for the 80–90% by its nucleus. According to literature data, twelve Raman bands were selected and used as markers for nucleic acids (5 marker bands), proteins (3 marker bands) and lipids (4 marker bands) components. Information about the distribution of nucleic acids, protein and lipids within each cell were gained by comparison of Raman marker bands. Furthermore, the average value of the intensities of four Raman spectra acquired in different regions of each cell was used to derive its metabolic state.

2.5. PCA analysis

To improve PCA analysis, all the spectra were previously subjected to some data treatment. First of all a continuous baseline correction was performed using the adaptive iteratively re-weighted penalized least square algorithm (airPLS) [12]. Corrected spectra were then normalized to their own area and slightly smoothed using the Savitzky–Golay smoothing-derivative procedure [13]. The resulting spectra were loaded into rows of a matrix, which was used as input for PCA and HCA procedures. PCA, HCA and all of the other data treatments were performed using custom scripts written in Matlab©.

2.6. Transmission electron microscopy analysis

The morphology of the cells was investigated by Transmission Electron Microscopy (TEM). A JEOL JEM-2010 analytical electron microscope (LaB6 electron gun and 70 kV accelerating voltage), equipped with a Gatan 794 Multi-Scan CCD camera for digital imaging, was used

for TEM analysis. A drop of the cells suspension in PBS buffer was placed on holey coated carbon copper grid and examined after evaporation of the buffer.

1. Results and discussion

1.1. U-937 cells in fresh culture

The average number of non-viable U937 cells was determined trough Trypan Blue and DAPI staining. Epifluorescence microscopic pictures showed that few cells (below 4%) in fresh culture evidenced irregularly-shaped nuclei associated to a spontaneous apoptotic process (see Fig. 1). A result confirmed both by flow cytometry analysis of isolated nuclei and by morphological analysis of hypo-diploid nuclei (data not shown), and in good agreement with a previous study [14].

A representative Raman spectrum of U-937 cells in fresh culture is shown in Fig. 2. The red line corresponds to the calculated mean spectrum averaged over all the Raman spectra acquired on the fresh culture, after baseline correction and smoothing. The gray shaded area is enclosed by standard deviation values limits. After the acquisition, no U937 cell showed evidence of damage in the proximity of irradiated area, neither interference by the culture media components was observed. In the U937 cells Raman spectra many peaks are observable and assignable to nucleic acids, proteins, carbohydrate and lipids. In particular, the contributions due to the DNA backbone vibrations are visible at 788 and 1095 cm^{-1} [15], that due to the DNA ring breathing mode is located at 678 cm^{-1} [16], while the features of the purine ring stretching and ring breathing modes of the DNA/RNA bases are found at 1582 cm^{-1} [15] and 1263 cm^{-1} [16], respectively. Moreover, representative bands ascribed to the protein peptide backbone vibrations are evident in the 1300–1680 cm^{-1} region: Amide I, Amide II and Amide III features are located at 1664 cm^{-1}, 1614 cm^{-1} and 1319 cm^{-1} [17–19], respectively. Amino acid contributions to the Raman spectrum were identified as due to tryptophan (at 759 cm^{-1}) [20], and tyrosine (at 830, 1172 and 1207 cm^{-1}) [21], while the characteristic band of phenylalanine, and expected at 1003 cm^{-1} is probably hidden by vibrational modes of carbohydrates groups in the 972–994 cm^{-1} spectral region, of ribose C–O group (at 994 cm^{-1}) [22] and of monosaccharides and disaccharides C–O–C groups (at 897 cm^{-1}) [23]. Finally, the U937 Raman spectrum is characterized by the presence of vibrational modes of lipid groups, at 1263, 1300 and 1439 cm^{-1} [20, 24], and phospholipid groups at 1656 [19] cm^{-1}. The phosphate group Raman signal, characteristic of most phospholipids, is observed at 860 cm^{-1} [25]. In Fig. 2 the calculated standard deviation values for these Raman peaks are reported, in percent.

Slight spectra variations from cell to cell were observed, probably associated to a different organization of bio-molecules within each cell, in a similar way to what has been observed in the Raman spectra of single, fixed lymphocytes [26]. Nevertheless, the fact that the probed area is smaller than the typical dimension of a single cell should also to be taken into account, as changes in the Raman spectra can arise if different structures inside the cells are probed. In order to ascertain this point, different regions within a single cell were probed. Nevertheless, within the same cells, Raman spectra recorded at different positions were similar, pointing out for the absence of evident intracellular variability, in agreement with the results of P.V. Zinin et al., establishing that proteins and lipids in U-937 cells are homogeneously distributed [27].

1.2. U-937 cells in aging culture

In all tested cultures, 144 h after the cells transfer into fresh culture vessels, a significant increase of apoptosis induction was observed by epifluorescence microscopy, a result confirmed by flow cytometry analysis (not reported here). After this time interval, about 20% of the cells on the average showed structural alterations of cellular nucleus, that can be associated to apoptotic features (see Fig. 3).

The observed structural modifications can be highlighted in the Raman spectra where spectral modifications in the aged culture were observed with respect to the U937 cell fresh culture. Modifications of the intensities of some Raman peaks can be observed at a glance in Fig. 4 where the mean Raman spectrum is reported in comparison with the fresh culture one (see Fig. 2). An overall increase of the standard deviation values for some peaks is evident. In particular in the low frequency side of the spectrum between 400 and 900 cm^{-1} and in the high frequency range between 1700 and 2000 cm^{-1}.

To further investigate this aspect, specific spectral regions [16,19,21, 23,24,28–30], correlated to the presence and concentration of specific bio-molecules within each cell, were selected and used as markers for nucleic acids, lipids and proteins (see Table 1).

In Fig. 5 the main intensities and the relative standard deviations of Raman peaks, classified as belonging to specific bio-molecules, are reported. As expected, the aged U937 are characterized by a larger cell-to-cell variability. It is well known that cell shape alterations and bleb formation are strikingly rapid phenomena. As it occurs, the irregular round shape of the living cells with many pseudopodia-like protrusions is replaced by a smooth round shape of apoptotic cells with protruding spherical-shaped blebs [31].

Optical and epifluorescence microscopy images were used to identify different morphological cell states. In particular two morphological types of U937 cells, named "*cell a*" and "*cell b*" were identified as

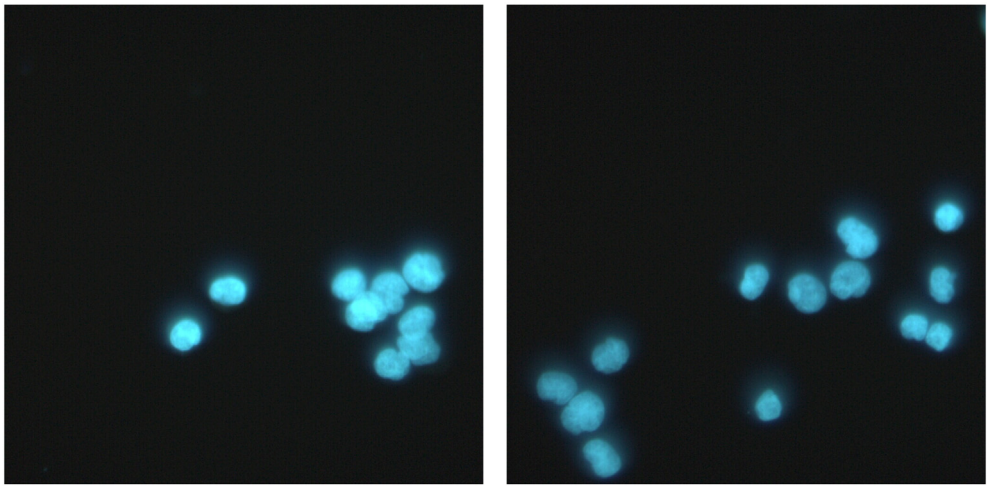

Fig. 1. Fluorescence imaging by DAPI staining of U937 cells in fresh culture.

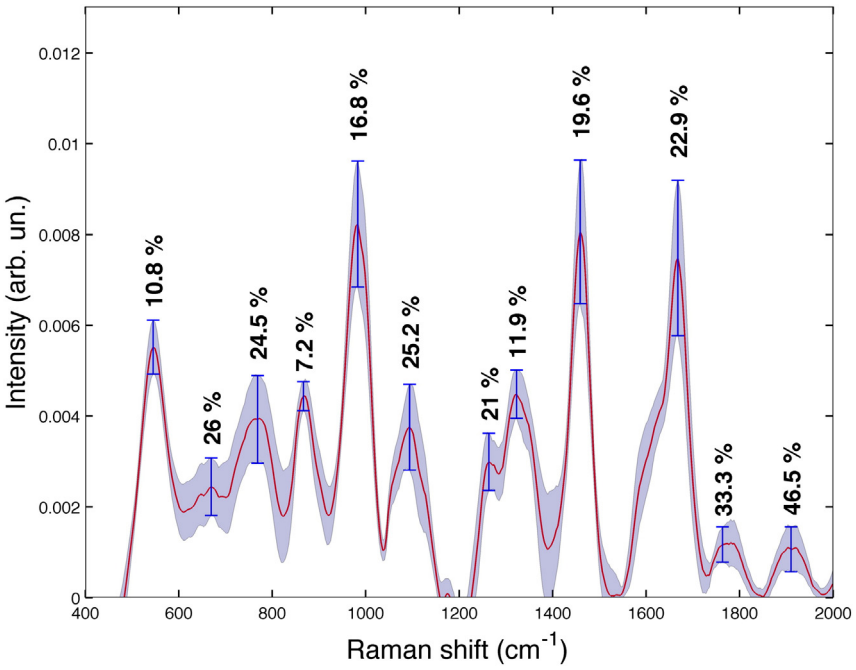

Fig. 2. Mean Raman spectrum and standard deviation values for U937 cell line in fresh culture. (For interpretation of the references to color in this figure, the reader is referred to the web version of this article.)

belonging to an apparently *healthy* and *apoptotic* state, respectively. For each cell type, three different areas were probed to check for Raman features spatial variations.

In Fig. 6, optical microscopy images of two different morphologies are shown, along with the corresponding Raman spectra acquired at three different positions as indicated in the optical images. The Raman intensities peaks, related to nucleic acids, proteins and lipids as a function of the probed position, are also reported.

Raman spectra acquired on the "*cell a*" showed a large spatial variations in the distribution of nucleic acids, proteins and lipids. This finding is in agreement with the unsynchronized metabolic condition of the U937 cell line, revealing both different concentration and distribution of bio-molecules within each cell. On the contrary "*cell b*" showed a lower spatial variation of the signals.

In Fig. 7 we report the mean intensity values of the Raman peaks averaged over the spectra acquired at different positions. As it can be seen *cell b* shows a significant decrease of the bands intensities corresponding to nucleic acids, compatible with phenomena of fragmentation of the DNA and other nuclear components, already observed by DAPI staining. A slight intensity increase of the features due to protein and lipids contributions is also observed, compatible with phenomena of chromatin condensation, different transcriptional activity, abnormal protein folding and accumulation of both membrane and non-membrane lipids (triglycerides).

Although these pictures could be with non-apoptotic mechanisms, such as autophagy, mitotic catastrophe and necrosis, these evidences are correlated to chromatin condensation (Fig. 8 up-left) and the formation of nuclear vesicles budding from the nucleus (Fig. 8 down-left).

TEM images (Fig. 8 right) show agglomerated nanostructures both outside the cells and engulfed in vesicles. All these morphological features are representative of cytoplasmic vacuolation (cyan arrow), nuclear vesicles budding from the nucleus (red arrows), as well as

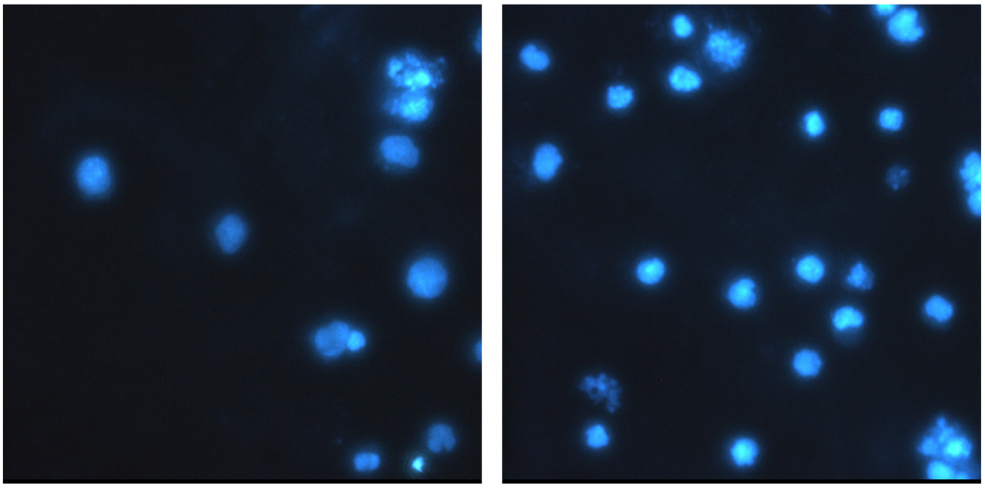

Fig. 3. Fluorescence imaging by DAPI staining of U937 cells in aging culture.

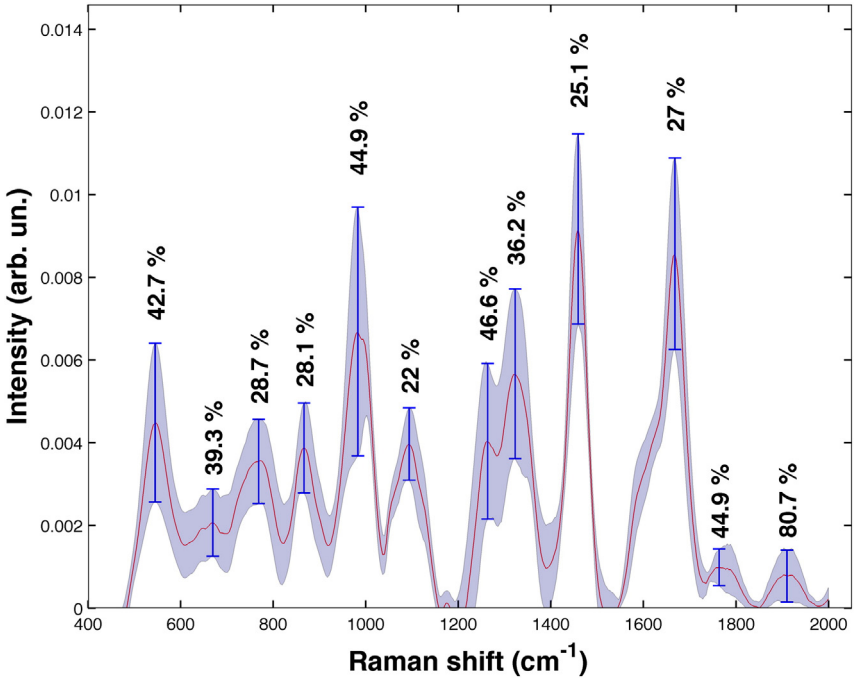

Fig. 4. Mean Raman spectrum and standard deviation values for U937 cell line in aging culture.

chromatin condensation (green arrows). On the overall, they are indicative of undergoing apoptotic cells [32], in good agreement with fluorescence data.

Moreover, in most of the late apoptotic stage cells, cytoplasm did not contain organelles, such as ribosomes or mitochondria, and scarce evidence of endoplasmic reticulum was observed at the bleb locations [31]. Raman signal at around 1760 cm^{-1} (see Fig. 9), usually attributed to cell internal cytomembrane and mitochondria [33], was absent, thus supporting the "*cell b*" apoptotic pattern.

On the basis of the previously discussed results, being the U937 cell line a model of leukemia, Raman spectroscopy can be potentially applied for monitoring the time evolution of sporadic tumor cells in different states of development. However, a faster and reproducible Raman spectra analysis method is needed both to identify tumoral cells and/or to follow the evolution of each cell (i.e. to determine whether the cell is in a divisional or in an apoptotic state).

To this purpose Raman spectra of U937 were analyzed by PCA. As an input set for the PCA and subsequent HCA procedures, the Raman spectra, after baseline subtraction area normalization and smoothing procedures, were used [34]. The result of a PCA analysis performed on a given data set is a vector which contains the relevance of principal components classified as a function of their variance. Usually, most of the variance is contained in the first three principal components PC 1, PC 2 and PC 3. Thereafter, HCA algorithm is applied to the PCA results in order to separate the data into statistically similar groups.

The results of the PCA analysis and of the subsequent HCA procedure are shown in Fig. 10 where the PC1 vs PC2 values are reported. The points enclosed in the two ellipsis refer to the two clusters, as they were identified by the HCA algorithm. The two clusters contain 10 (cluster#1) and 3 (cluster#2) spectra respectively. More than the 80% of the variance is within the first two principal components (PC1 and PC2) and the two clusters are well separated from each other, pointing out for the presence of clear differences in the Raman spectra of the two groups. These differences can be clearly seen when looking at the mean spectra of the two clusters shown in Fig. 10, obtained averaging over all the spectra belonging to the clusters. The most striking differences between the two clusters are in the low frequency region, between 400 and 1200 cm^{-1}, and in the high frequency region above 1700 cm^{-1}. In the low frequency region all the Raman peaks that were previously discussed and assigned are present in both clusters, but the intensities

Table 1
Main Raman marker bands for nucleic acids, lipids and proteins.

Region	Raman marker bands (cm^{-1})	Vibrational modes	Assignments	Ref.
Nucleic acids	775–803	Nucleotide ring breathing	DNA bases	[24]
	811–13	Distinct peak	RNA	[16]
	1093–97	O–P–O backbone stretching	DNA	[16]
	1370–74	Ring breathing modes	DNA/RNA bases	[16]
	1576–78	Vibrational mode	Nucleic acids	[28]
Lipids	1263–64	β(═CH)	Lipids bond	[24]
	1300–03	$\tau(CH_2)$	Lipids bond	[19]
	1439–42	$\beta(CH_2)$	Lipids bond	[19]
	1650–57	ν(C═C) cis	Phospholipids	[19]
		C═C	Lipids	
Proteins	1315–30	Amide III (α-helix)	Protein peak	[19]
	1450–1458	Aliphatic side groups	Amino acid residues	[29,30]
		CH2 bending mode and scissoring	Proteins	
		Amide III (CH_2 deformation)	Protein peak	
	1658–71	ν(C═O) stretching Amide I,	Protein peak	[21,23,30]
		β-pleated sheet or random coil conformation		

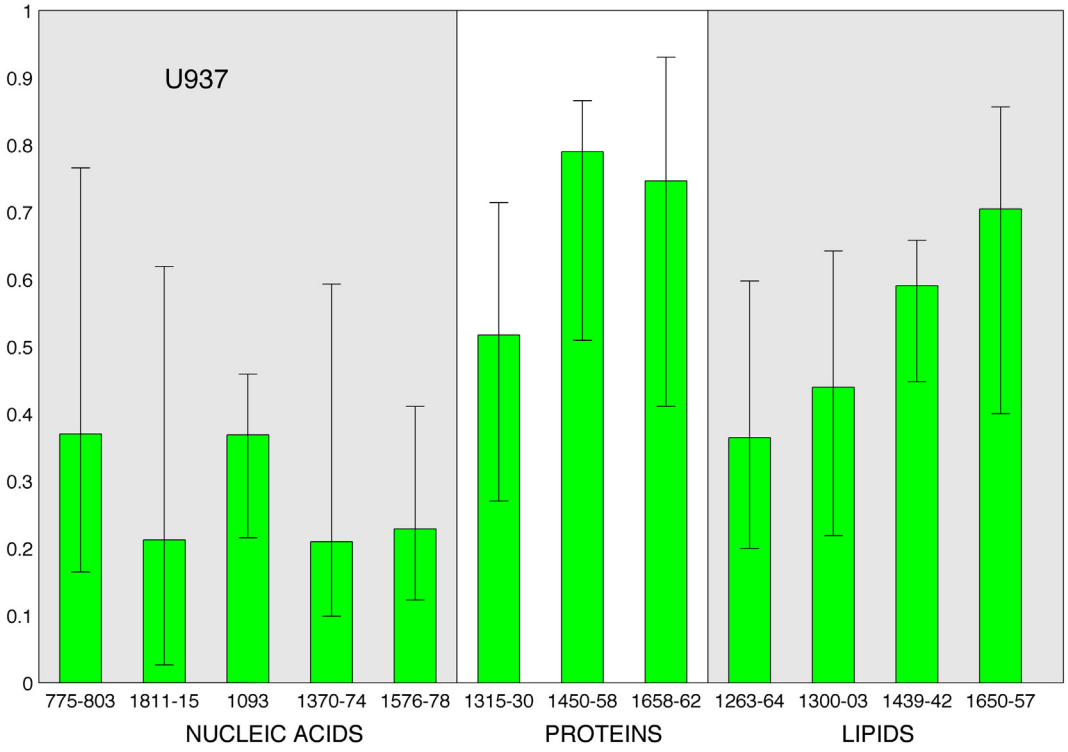

Fig. 5. Intensity variability of Raman marker bands for U937 cell line in aging culture.

of the Raman peaks in cluster#2 are clearly lower than the cluster#1 ones. When comparing these intensities we take the height of the most intense Raman peak (at 1450 cm^{-1}) as a reference. In the high frequency region two peaks are missing in the averaged spectrum of cluster#2, i.e. the two at 1760 and 1900 cm^{-1}. These differences correspond to the ones observed in "*cell a*" and "*cell b*" as previously discussed and reported in Fig. 9. Thus, PCA can discriminate, within a cell line, not only differences due to the normal or cancerous cell state but also among the normal, stressed or apoptotic states of the cells too. Such an occurrence should be taken into account when using PCA as a diagnostic tools without an analysis of the cells Raman spectra.

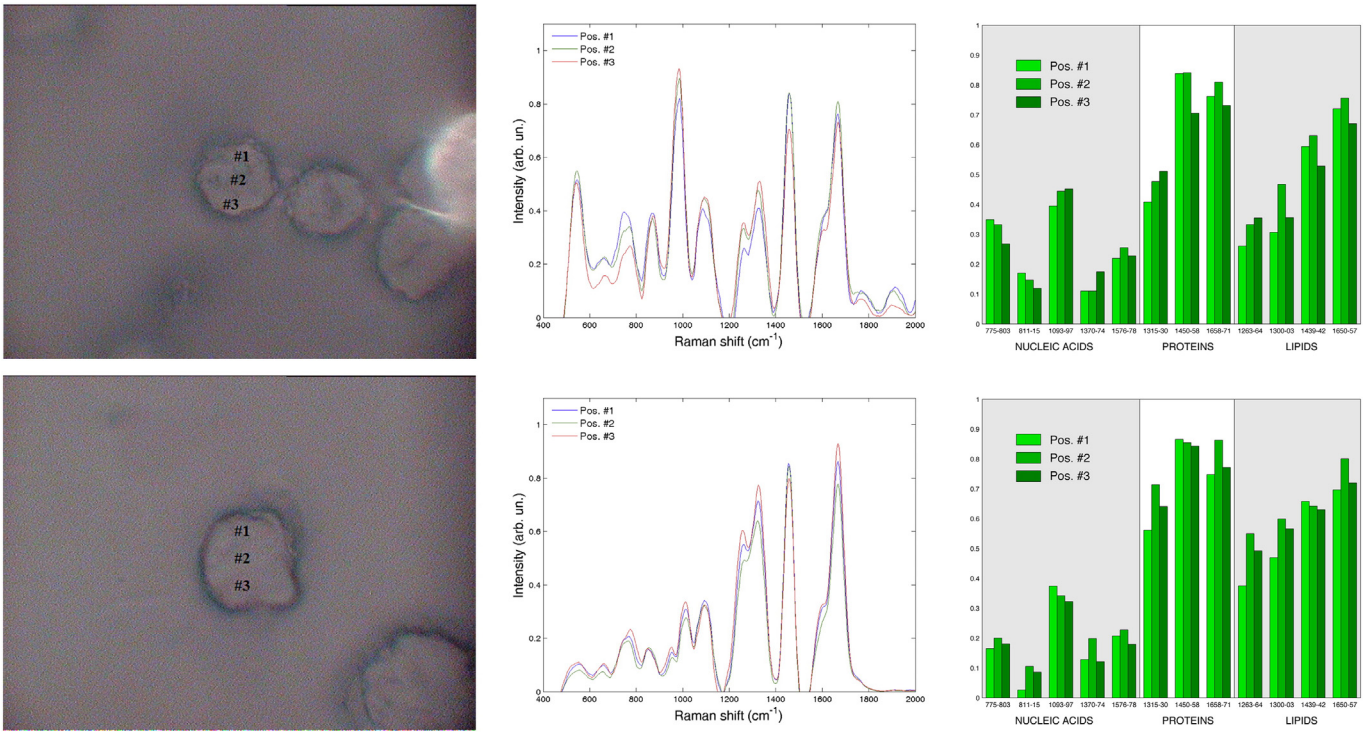

Fig. 6. Optic microscopy images (left), Raman spectra (center) and spatial distribution of Raman marker bands for "*cell a*" (up) and "*cell b*" (down) by aging culture.

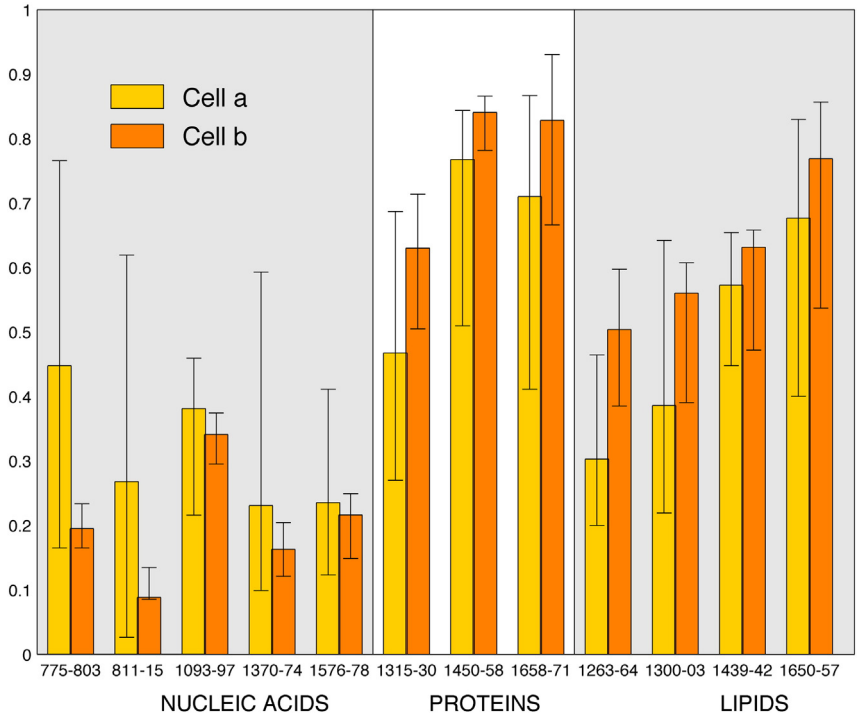

Fig. 7. Intensity variability of Raman marker bands for "*cell a*" and "*cell b*" by aging culture.

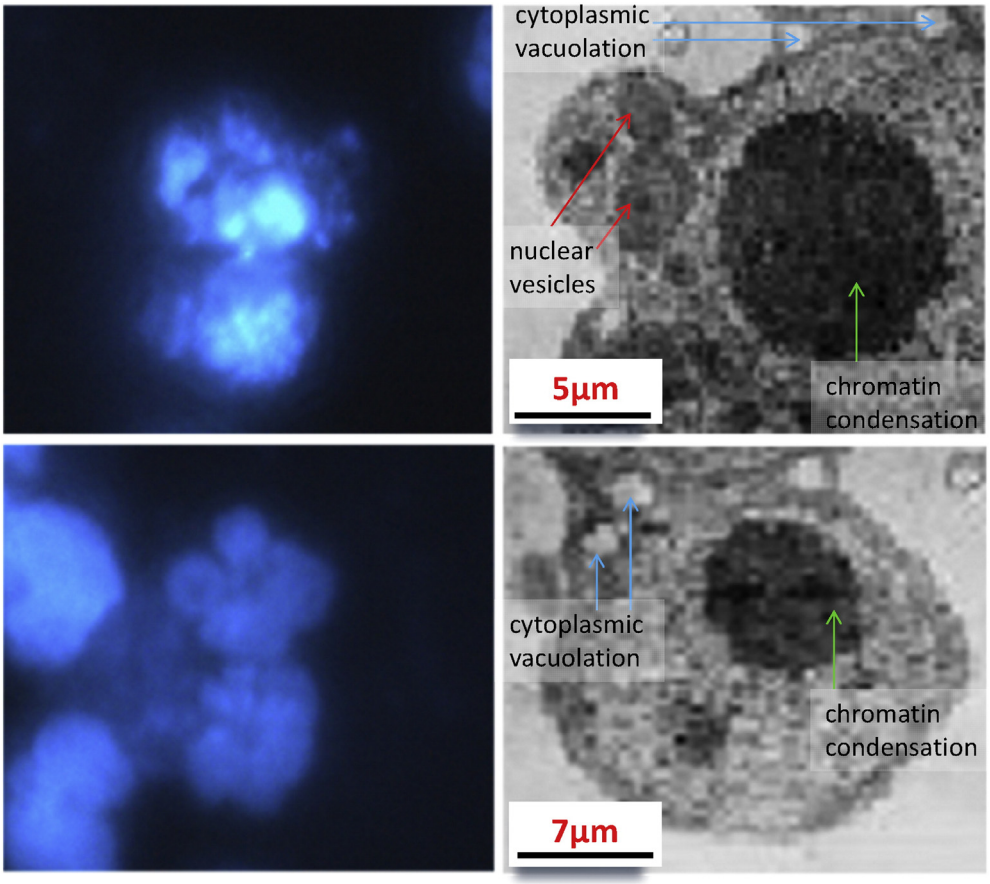

Fig. 8. Fluorescence imaging by DAPI staining (left) and TEM images (right) of U937 cells in aging culture.

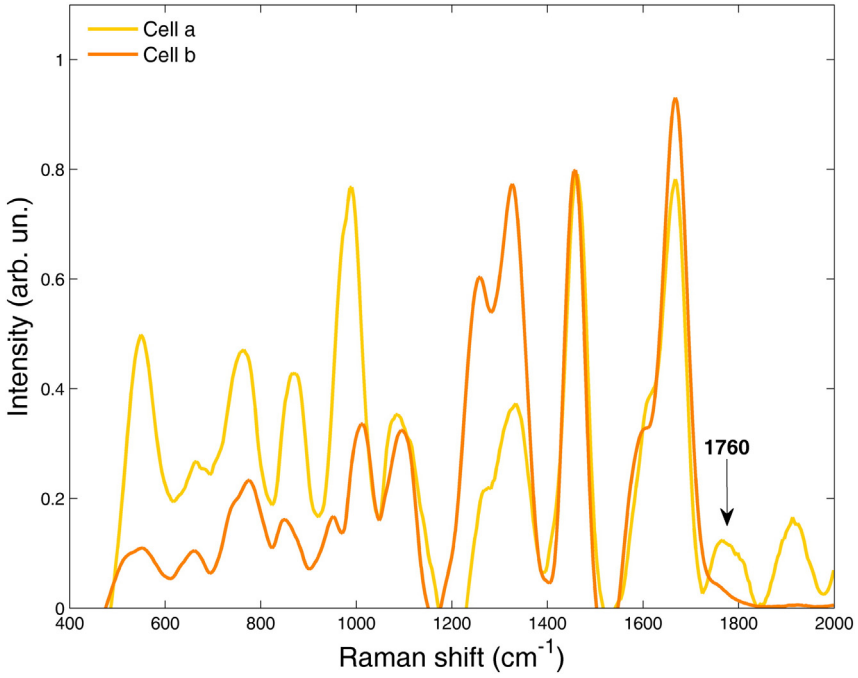

Fig. 9. Representative Raman spectra of U937 cell in undefined ("*cell a*") and clear apoptotic ("*cell b*") metabolic states.

2. Conclusions

It is well known that a large genetic heterogeneity exists not only among different kind of cancer but also among cells of a specific cancer. The high rate of genetic variations characterizes the progression of some cancers, and in particular of some leukemias, leading to a high degree of cellular diversification. However, the presence of multiple clusters for the same cell line, in dependence of the different metabolic states, may result in a difficult identification of the same tumor cell line. This might lead to think that, when evaluating different cells, especially when taken by different patients, it may be expected that Raman spectra variability would greatly increase. The knowledge and the characterization of such complex phenomena are of paramount importance in order to establish a personalized and effective cancer therapy.

To address these questions, we explored the use of micro-Raman spectroscopy as a tool for "real time" monitoring of the cancer cell evolution and diversification.

To this purpose, the time evolution of healthy U937 cell cultures have been analyzed to address the effects, including necrosis and apoptosis, induced by aging stress.

Optical and epifluorescence imaging were used to gain information about healthy or apoptotic cell status the results were correlated to a detailed analysis of the spectral Raman features. PCA analysis performed on Raman spectra was able to distinguish evident apoptotic cells from the others, demonstrating that molecular modifications within the same cell line can be highlighted; our results show that these two distinct conditions are correctly identified by PCA plot.

We propose the use of the analysis of specific spectral areas, within the available spectral range, relating to nucleic acids,

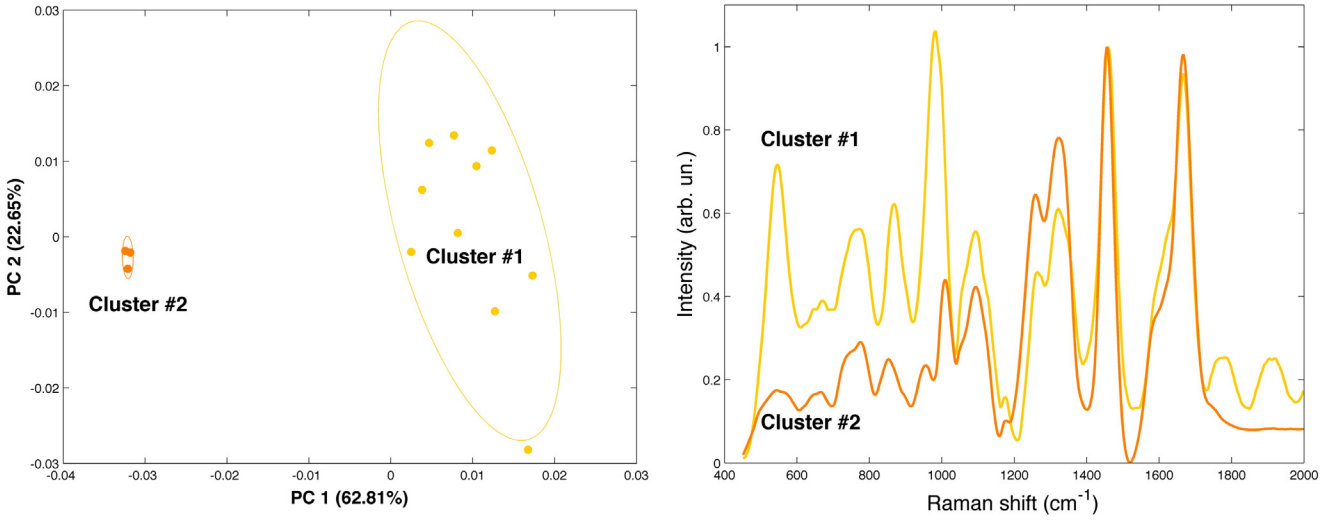

Fig. 10. a) PCA plot (PC2 vs PC1) obtained using the Raman spectra of aged (144 h) U937 cells, ellipses indicate 85% confidence limits; b) mean spectra of the two clusters identified by the HCA procedure performed on the output of the PCA.

proteins and lipids, as spectral biomarkers of metabolic state that help to clarify the evolutionary events within the same tumor cell line. Specific bands were assigned and used to identify critical features able to discriminate between spectra of healthy and apoptotic cells.

Potentially, this type of survey may be also extended to analyze possible heterogeneities arising during tumor progression and/or therapy resistance, leading to significant advances in leukemia care and eradication of minimal residual diseases. In particular, these data can help to correctly identify the presence of sporadic tumor cells in different states of development, as during chemotherapy or, for instance, when estimating the minimal residual disease after chemotherapeutic treatment.

Acknowledgments

Authors gratefully acknowledge A.B.A.L. onlus Messina (Italy) (http://www.abalmessina.it) for the use of the XploRA Raman spectrometer. This work was partially funded by Italian Ministry of Education, University and Research (MIUR) by means of the national Program PON R&C 2007–2013, project "Hyppocrates–Sviluppo di Micro e Nano-Tecnologie e Sistemi Avanzati per la Salute dell'Uomo (PON02 00355)".

References

[1] M. Greaves, C.C. Maley, Clonal evolution in cancer, Nature 481 (2012) 306–313, http://dx.doi.org/10.1038/nature10762.
[2] N. Stone, C. Kendell, N. Shepherd, P. Crow, H. Barr, Near-infrared Raman spectroscopy for the classification of epithelial pre-cancers and cancers, J. Raman Spectrosc. 33 (2002) 564–573, http://dx.doi.org/10.1002/jrs.882.
[3] G. Lentini, E. Fazio, F. Calabrese, L.M. De Plano, M. Puliafico, D. Franco, M.S. Nicolò, S. Carnazza, S. Trusso, A. Allegra, F. Neri, C. Musolino, S.P.P. Guglielmino, Phage-AgNPs complex as SERS probe for U937 cell identification, Biosens. Bioelectron. 74 (2015) 398–405, http://dx.doi.org/10.1016/j.bios.2015.05.073.
[4] P.R. Carey, Raman spectroscopy, the sleeping giant in structural biology, awakes, J. Biol. Chem. 274 (1999) 26625–26628, http://dx.doi.org/10.1074/jbc.274.38.26625.
[5] U. Neugebauer, J.H. Clement, T. Bocklitz, C. Krafft, J. Popp, Identification and differentiation of single cells from peripheral blood by Raman spectroscopic imaging, J. Biophotonics 3 (2010) 579–587, http://dx.doi.org/10.1002/jbio.201000020.
[6] V. Ranc, J. Srovnal, L. Kvítek, M. Hajduch, Discrimination of circulating tumor cells of breast cancer and colorectal cancer from normal human mononuclear cells using Raman spectroscopy, Analyst 138 (2013) 5983–5988, http://dx.doi.org/10.1039/c3an00855j.
[7] I.S. Patel, W.R. Premasiri, D.T. Moir, L.D. Ziegler, Barcoding bacterial cells: a SERS based methodology for pathogen identification, J. Raman Spectrosc. 39 (2008) 1660–1672, http://dx.doi.org/10.1002/jrs.2064.
[8] S. Boydston-White, M. Romeo, T. Chernenko, A. Regina, M. Miljković, M. Diem, Cell-cycle-dependent variations in FTIR micro-spectra of single proliferating HeLa cells: principal component and artificial neural network analysis, Biochim. Biophys. Acta 1758 (2006) 908–914, http://dx.doi.org/10.1016/j.bbamem.2006.04.018.
[9] E. Brauchle, S. Thude, S.Y. Brucker, K. Schenke-Layland, Cell death stages in single apoptotic and necrotic cells monitored by Raman microspectroscopy, Sci. Rep. 4 (2014) 4698, http://dx.doi.org/10.1038/srep04698.
[10] C. Sundstrom, K. Nilsson, Establishment and characterization of a human histiocytic lymphoma cell line (U-937), Int. J. Cancer 17 (5) (1976) 565–577, http://dx.doi.org/10.1002/ijc.2910170504.
[11] G. Clark, Staining Procedures, fourth ed., 1981 49–91.
[12] A. Savitzky, M.J.E. Golay, Smoothing and differentiation of data by simplified least squares procedures, Anal. Chem. 36 (1964) 1627–1639, http://dx.doi.org/10.1021/ac60214a047.
[13] Z.M. Zhang, S. Chen, Y.Z. Liang, Baseline correction using adaptive iteratively reweighted penalized least squares, Analyst 135 (2010) 1138–1146, http://dx.doi.org/10.1039/b922045c.
[14] A. Mastino, M.T. Sciortino, M.A. Medici, D. Perri, M.G. Ammendolia, S. Grelli, C. Amici, A. Pernice, S.P.P. Guglielmino, Herpes simplex virus 2 causes apoptotic infection in monocytoid cells, Cell Death Differ. 4 (1997) 629–638, http://dx.doi.org/10.1038/sj.cdd.4400289.
[15] P.R. Jess, D.D. Smith, M. Mazilu, K. Dholakia, A.C. Riches, C.S. Herrington, Early detection of cervical neoplasia by Raman spectroscopy, Int. J. Cancer 121 (2007) 2723–2728, http://dx.doi.org/10.1002/ijc.23046.
[16] J.W. Chan, D.S. Taylor, T. Zwerdling, S.T. Lane, K. Ihara, T. Huser, Micro-Raman spectroscopy detects individual neoplastic and normal hematopoietic cells, Biophys. J. 90 (2) (2006) 648–656, http://dx.doi.org/10.1529/biophysj.105.066761.
[17] Y. Yang, J. Sule-Suso, G.D. Sockalingum, G. Kegelaer, M. Manfait, A.J. El Haj, Study of tumor cell invasion by Fourier transform infrared microspectroscopy, Biopolymers 78 (2005) 311–317, http://dx.doi.org/10.1002/bip.20297.
[18] E.O. Faolain, M.B. Hunter, J.M. Byrne, P. Kelehan, M. McNamer, H.J. Byrne, F.M. Lyng, A study examining the effects of tissue processing on human tissue sections using vibrational spectroscopy, Vib. Spectrosc. 38 (2005) 121–127, http://dx.doi.org/10.1016/j.vibspec.2005.02.013.
[19] R.J. Lakshimi, V.B. Kartha, C.M. Krishna, J.G.R. Solomon, G. Ullas, P. Uma Devi, Tissue Raman spectroscopy for the study of radiation damage: brain irradiation of mice, Radiat. Res. 157 (2002) 175–182, http://dx.doi.org/10.1667/0033-7587(2002)157[0175:TRSFTS]2.0.CO;2.
[20] N. Stone, C. Kendall, J. Smith, P. Crow, H. Barr, Raman spectroscopy for identification of epithelial cancers, Faraday Discuss. 126 (2004) 141–157, http://dx.doi.org/10.1039/b304992b.
[21] W.T. Cheng, M.T. Liu, H.N. Liu, S.Y. Lin, Micro-Raman spectroscopy used to identify and grade human skin pilomatrixoma, Microsc. Res. Tech. 68 (2005) 75–79, http://dx.doi.org/10.1002/jemt.20229.
[22] G.I. Dovbeshko, N.Y. Gridina, E.B. Kruglova, O.P. Pashchuk, FTIR spectroscopy studies of nucleic acid damage, Talanta 53 (2000) 233–246, http://dx.doi.org/10.1016/S0039-9140(00)00462-8.
[23] G. Shetty, C. Kedall, N. Shepherd, N. Stone, H. Barr, Raman spectroscopy: elucidation of biochemical changes in carcinogenesis of oesophagus, Br. J. Cancer 94 (2006) 1460–1464, http://dx.doi.org/10.1038/sj.bjc.6603102.
[24] R.E. Kast, G.K. Serhatkulu, A. Cao, A.K. Pandya, H. Dai, J.S. Thakur, V.M. Naik, R. Naik, M.D. Klein, G.W. Auner, R. Rabah, Raman spectroscopy can differentiate malignant tumors from normal breast tissue and detect early neoplastic changes in a mouse model, Biopolymers 89 (2008) 235–241, http://dx.doi.org/10.1002/bip.
[25] C. Krafft, L. Neudert, T. Simat, R. Salzer, Near-infrared Raman spectra of human brain lipids, Spectrochim. Acta A Mol. Biomol. Spectrosc. 61 (2005) 1529–1535, http://dx.doi.org/10.1016/j.saa.2004.11.017.
[26] N. Uzunbajakava, A. Lenferink, Y. Kraan, E. Volokhina, G. Vrensen, J. Greve, C. Otto, Nonresonant confocal Raman imaging of DNA and protein distribution in apoptotic cells, Biophys. J. 84 (2003) 3968–3981, http://dx.doi.org/10.1016/S0006-3495(03)75124-8.
[27] P.V. Zinin, A. Misra, L. Kamemoto, Q. Yu, N. Hu, S.K. Sharma, Visible, near-infrared, and ultraviolet laser-excited Raman spectroscopy of the monocytes/macrophages (U937) cells, J. Raman Spectrosc. 41 (2010) 268–274, http://dx.doi.org/10.1002/jrs.2444.
[28] S.C. Pinzaru, L.M. Andronie, I. Domsa, O. Cozar, S. Astilean, Bridging biomolecules with nanoparticles: surface-enhanced Raman scattering from colon carcinoma and normal tissue, J. Raman Spectrosc. 39 (2008) 331–334, http://dx.doi.org/10.1002/jrs.1907.
[29] S.K. Teh, W. Zheng, K.Y. Ho, M. Teh, K.G. Yeoh, Z. Huang, Diagnostic potential of near-infrared Raman spectroscopy in the stomach: differentiating dysplasia from normal tissue, Br. J. Cancer 98 (2008) 457–465, http://dx.doi.org/10.1038/sj.bjc.6604176.
[30] P. Cipriani, C.Y. Smith, Characterization of thalidomide using Raman spectroscopy, Spectrochim. Acta A Mol. Biomol. Spectrosc. 69 (2008) 333–337, http://dx.doi.org/10.1016/j.saa.2007.04.002.
[31] E. Bonannol, M. Ruzittu, E.C. Carlà, M.R. Montinari, P. Pagliara, L. Dini, Cell shape and organelle modification in apoptotic U937 cells, Eur. J. Histochem. 44 (3) (2000) 237–246 (ISSN: 1121-760X).
[32] P. Mita, A. De Luca, L. Abbro, L. Dini, Ultrastructural analysis of apoptosis induced by apoptotic U937 cells conditioned medium, Ital. J. Zool. 70 (2003) 141–146, http://dx.doi.org/10.1080/11250000309356507.
[33] K. Mitra, C. Wunder, B. Roysam, G. Lin, J. Lippincott-Schwartz, A hyperfused mitochondrial state achieved at G1-S regulates cyclin E buildup and entry into S phase, Proc. Natl. Acad. Sci. U. S. A. 106 (2009) 11960–11965, http://dx.doi.org/10.1073/pnas.0904875106.
[34] A. Taleb, J. Diamond, J.J. McGarvey, J.R. Beattie, C. Toland, P.W. Hamilton, Raman microscopy for the chemometric analysis of tumor cells, J. Phys. Chem. B 110 (2006) 19625–19631, http://dx.doi.org/10.1021/jp061981q.